

# Molecular dynamics simulations of vacancy diffusion in chromium(III) oxide, hematite, magnetite and chromite

Jukka Vaari \*

VTT Technical Research Centre of Finland, Kemistintie 3, P.O. Box 1000, FI-02044 VTT, Finland



## ARTICLE INFO

### Article history:

Received 27 June 2014

Received in revised form 25 November 2014

Accepted 27 November 2014

Available online xxxx

### Keywords:

Molecular dynamics

Mass transport

Migration energy

Schottky defects

## ABSTRACT

Mass transport in bulk  $\alpha$ -Cr<sub>2</sub>O<sub>3</sub>,  $\alpha$ -Fe<sub>2</sub>O<sub>3</sub>, Fe<sub>3</sub>O<sub>4</sub> and FeCr<sub>2</sub>O<sub>4</sub> has been studied by means of classical molecular dynamics (MD) simulations. Point defects were assumed to be responsible for ionic diffusion. The focus of this study were vacancies both in the cation and anion lattice (Schottky defects). The Buckingham potential was used to describe the interactions between ions. Defect concentrations in the  $10^{-4}$  to  $10^{-3}$  range were studied in the temperature range 1300 K–2000 K. Diffusion coefficients were calculated from mean square displacements. Activation energies for migration were determined from Arrhenius plots.

© 2014 Elsevier B.V. All rights reserved.

## 1. Introduction

Mass transport properties of metal oxides have attracted much experimental, theoretical and computational attention due to the importance of a surface oxide layer in determining the lifetime of metallic components in a wide range of applications. The oxides investigated in this work are typically formed on the surface of a low-alloy steel during exposure to high-temperature oxidative environments, as exemplified by Fig. 1 [1]. This shows the outward diffusion of iron to form the outer oxide consisting of magnetite and hematite layers and inward diffusion of oxygen together with enrichment of Cr to form the mixed hematite-chromite inner layer. The aim in this work is to provide insight, using atomistic simulation methods, on the details of the diffusion processes involved.

Despite the prevalence of these oxides, we have found surprisingly little work done using atomistic simulation methods related to the mass transport properties. Catlow et al. [2] determined lattice and electronic defect formation and migration energies for  $\alpha$ -Cr<sub>2</sub>O<sub>3</sub> and  $\alpha$ -Fe<sub>2</sub>O<sub>3</sub>, based on a Mott–Littleton approach. Later, Atkinson et al. [3] extended the approach to include lattice defects induced by impurities. Direct MD simulations on bulk diffusion for these materials seem to be missing. However, MD simulations have been reported on the ordering of  $\alpha$ -Cr<sub>2</sub>O<sub>3</sub>(0001) surface [4,5].

One complicating factor related to MD work is the complex defect chemistry of these oxides, yielding a large number of possible initial configurations for the simulations. The defect chemistry is affected

both by impurities as well as the sample preparation procedure. Holt and Kofstad [6] report elevated levels of Mg and Al impurities in their Cr<sub>2</sub>O<sub>3</sub> samples due to extended exposure to the materials in the conductivity measuring instruments. According to Atkinson et al. [3], small divalent substitutional cations (such as Mg) in a Cr<sub>2</sub>O<sub>3</sub> lattice have solution energies of the order of 2 eV, significantly less than the energies of intrinsic defect formation. This implies that real Cr<sub>2</sub>O<sub>3</sub> samples should be regarded as doped semiconductors with the charge carrier concentration dictated by the impurity concentration.

The focus in this study is diffusion due to point defects. However, even the nature of the dominant point defect type in the oxides of this study is not always fully agreed on. For example, Su and Simkovich [7] present a comprehensive analysis on the point defect structure of Cr<sub>2</sub>O<sub>3</sub> fully starting out from the assumption that the point defects are in the cation lattice. Young et al. [8] acknowledge the possibility of defects in the oxygen lattice to explain the observed p-type conductivity in their Cr<sub>2</sub>O<sub>3</sub> samples but go on to conclude that Cr lattice defects are a more plausible explanation. Holt and Kofstad [9], in a study of Mg-doped Cr<sub>2</sub>O<sub>3</sub>, discuss the possibility of defects in the oxygen lattice, a conclusion supported by the calculations by Atkinson et al. [3].

We will entirely concentrate on Schottky-type point defects. Energetics and mechanisms of defect formation will not be studied. Instead, pre-defined defect concentrations will be used. The defect concentrations used in the simulations are in the  $10^{-4}$  to  $10^{-3}$  range in order to ensure minimal interaction between individual defects and to avoid defect clustering. Simulations are conducted in temperature range 1300 K–2000 K in order to determine the activation energy of migration.

\* Tel.: +358 40 5233692.

E-mail address: [jukka.vaari@vtt.fi](mailto:jukka.vaari@vtt.fi).

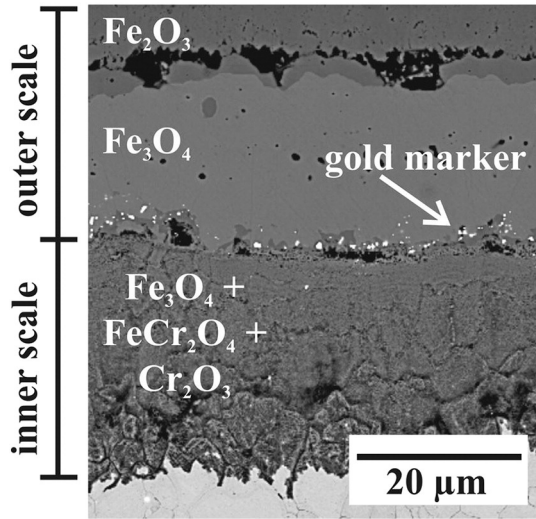


**Fig. 1.** Oxide scale on a low alloy steel (grade  $\times 60$ ) after exposure at 550 °C to laboratory air for 72 h.

## 2. Computational details

The atomic interactions in this work were described by a Buckingham potential in combination with a Coulomb term:

$$V_{ij}(r_{ij}) = A_{ij} \exp\left(-\frac{r_{ij}}{\rho_{ij}}\right) - \frac{C_{ij}}{r_{ij}^6} + \frac{q_i q_j}{r_{ij}}$$

The parameters used in the simulations are shown in Table 1. Two different parameters sets applicable to  $\alpha$ -Cr<sub>2</sub>O<sub>3</sub> and  $\alpha$ -Fe<sub>2</sub>O<sub>3</sub> were used. Pairwise interactions were explicitly calculated up to a distance of 15 Å. Long-range Coulombic interactions were computed by the Ewald method. Polarization effects were not accounted for. Only Coulombic interaction was assumed between cations due to the small radius of these ions. All ions were assumed to adopt their formal charges.

For  $\alpha$ -Cr<sub>2</sub>O<sub>3</sub> and  $\alpha$ -Fe<sub>2</sub>O<sub>3</sub>, a supercell of  $20 \times 20 \times 10$  hexagonal unit cells with periodic boundary conditions was used in the simulations for a total of 120000 atoms. For Fe<sub>3</sub>O<sub>4</sub> and FeCr<sub>2</sub>O<sub>4</sub>, a supercell of  $15 \times 15 \times 15$  cubical unit cells (189000 atoms) with periodic boundary conditions was used. In the case of Fe<sub>3</sub>O<sub>4</sub> reverse spinel, one Fe<sup>3+</sup> cation was placed in the tetrahedral site, and the remaining Fe<sup>3+</sup> cation and the Fe<sup>2+</sup> cation were randomly distributed in the octahedral holes. Schottky defects

were generated by randomly deleting atoms from both cation and anion lattices to maintain charge neutrality. The integration of Newton's equations was performed by the Verlet algorithm. A time step of 1.0 fs was used. All simulations were conducted in the NPT ensemble. Simulations were typically run up to 400 ps ( $\alpha$ -Cr<sub>2</sub>O<sub>3</sub> and  $\alpha$ -Fe<sub>2</sub>O<sub>3</sub>) of 600 ps (Fe<sub>3</sub>O<sub>4</sub> and FeCr<sub>2</sub>O<sub>4</sub>) of real time.

The diffusion of ions was measured by recording the mean square displacement (MSD) for ion type  $i$  as a function of time, and computing the diffusion constant from the slope of the MSD( $t$ ) curve according to

$$\langle r_i^2(t) \rangle = \frac{1}{N} \sum_N [r_i(t) - r_i(0)]^2 = 6Dt$$

To obtain the slope, a line was fitted to the MSD( $t$ ) curve from 200 ps to 400 ps for  $\alpha$ -Cr<sub>2</sub>O<sub>3</sub> and  $\alpha$ -Fe<sub>2</sub>O<sub>3</sub>, and from 200 ps to 600 ps for Fe<sub>3</sub>O<sub>4</sub> and FeCr<sub>2</sub>O<sub>4</sub>.

The MD simulations were performed using LAMMPS software [10].

## 3. Results

Simulations for  $\alpha$ -Cr<sub>2</sub>O<sub>3</sub> and  $\alpha$ -Fe<sub>2</sub>O<sub>3</sub> were performed for defect concentrations of  $8.3 \times 10^{-5}$ ,  $2.0 \times 10^{-4}$ ,  $4.2 \times 10^{-4}$  and  $8.3 \times 10^{-4}$  and for temperatures from 1300 K to 2000 K at 100 K intervals. The defects were created at 300 K, followed by a 10 ps heating time from 300 K to the target temperature. Fig. 2 presents typical MSD( $t$ ) curves from the simulations for  $\alpha$ -Cr<sub>2</sub>O<sub>3</sub>. The time zero in the figure has been set to the point in time when the simulation has reached the target temperature. This explains the initial non-zero MSD values, which are slightly different for the two parameter sets. The data contain considerable noise due to the low defect concentration, limiting the accuracy of determining the slope of the MSD( $t$ ) curve especially at lower temperatures. The main difference between the parameter sets is that for set 1, oxygen appears to be the mobile ion, while chromium shows essentially no diffusion. For set 2, both ions are mobile. Since both chromium and oxygen are experimentally known to be mobile species [6,14], parameter set 2 is believed to better represent mass diffusion in  $\alpha$ -Cr<sub>2</sub>O<sub>3</sub>.

It can be observed from Fig. 2 that for parameter set 2, the initial 10 ps heating period is not sufficient to equilibrate the system. The shape of the MSD curves is curved up to about 200 ps, after which a linear trend continues. This is the reason for determining diffusion coefficients from the MSD data after 200 ps.

The diffusion coefficients determined from the simulations for  $\alpha$ -Cr<sub>2</sub>O<sub>3</sub> at a Schottky defect concentration of  $8.3 \times 10^{-4}$  are presented in Fig. 3. Chromium data for parameter set 1 are not presented, as the MSD curves for chromium showed no slope that could have been determined reliably even at a temperature of 2000 K. The data (especially for Cr) contain scatter, which can be partly understood by the noise in the raw MSD data due to the low defect concentration, as exemplified by Fig. 2. Other sources of scatter include the initial defect configuration and the initial velocity distribution. To investigate the effect of the two latter sources, simulations with parameter set 2 were repeated by varying both the defect configuration and the initial velocity distribution. For  $T = 1600$  K, a total of five simulations were conducted. The results suggest that the initial configuration has an important effect on the determination of the diffusion coefficient. For oxygen, the migration activation energy and the values of the diffusion coefficient agree fairly well between the two parameterizations of the interaction potential.

The diffusion coefficients determined from the simulations for  $\alpha$ -Fe<sub>2</sub>O<sub>3</sub> at a Schottky defect concentration of  $8.3 \times 10^{-4}$  are presented in Fig. 4. In this case, it can be noted that both parameter sets predict mobility for both the anion and the cation, in agreement with the experimental findings by Amami et al. [15]. As with  $\alpha$ -Cr<sub>2</sub>O<sub>3</sub>, the scatter in the cation data is larger than for anion. No repeated simulations were carried out for  $\alpha$ -Fe<sub>2</sub>O<sub>3</sub>; however, for parameter set 2, additional data were obtained for temperatures of 1350 K, 1450 K and 1550 K. For Fe, the two parameter sets predict practically the same activation energy

**Table 1**  
Buckingham potential parameterizations used in this work.

| Oxide                                  | Interaction                       | A (eV)  | r (Å)  | C (eV·Å <sup>6</sup> ) | Reference |
|--|-----------------------------------|---------|--------|------------------------|-----------|
| Cr <sub>2</sub> O <sub>3</sub> , set 1 | Cr <sup>3+</sup> –O <sup>2–</sup> | 1734.1  | 0.301  | 0                      | [11]      |
|  | O <sup>2–</sup> –O <sup>2–</sup>  | 22764   | 0.149  | 27.88                  | [12]      |
| Cr <sub>2</sub> O <sub>3</sub> , set 2 | Cr <sup>3+</sup> –O <sup>2–</sup> | 1204.18 | 0.3165 | 0                      | [13]      |
|  | O <sup>2–</sup> –O <sup>2–</sup>  | 9547.96 | 0.2192 | 32                     | [13]      |
| Fe <sub>2</sub> O <sub>3</sub> , set 1 | Fe <sup>3+</sup> –O <sup>2–</sup> | 1102.4  | 0.3299 | 0                      | [11]      |
|  | O <sup>2–</sup> –O <sup>2–</sup>  | 22764   | 0.149  | 27.88                  | [12]      |
| Fe <sub>2</sub> O <sub>3</sub> , set 2 | Fe <sup>3+</sup> –O <sup>2–</sup> | 1414.6  | 0.3128 | 0                      | [13]      |
|  | O <sup>2–</sup> –O <sup>2–</sup>  | 9547.96 | 0.2192 | 32                     | [13]      |
| Fe <sub>3</sub> O <sub>4</sub>         | Fe <sup>3+</sup> –O <sup>2–</sup> | 1414.6  | 0.3128 | 0                      | [13]      |
|  | Fe <sup>2+</sup> –O <sup>2–</sup> | 649.1   | 0.3399 | 0                      | [11]      |
| FeCr <sub>2</sub> O <sub>4</sub>       | O <sup>2–</sup> –O <sup>2–</sup>  | 9547.96 | 0.2192 | 32                     | [13]      |
|  | Cr <sup>3+</sup> –O <sup>2–</sup> | 1204.18 | 0.3165 | 0                      | [13]      |
|  | Fe <sup>2+</sup> –O <sup>2–</sup> | 649.1   | 0.3399 | 0                      | [11]      |
|  | O <sup>2–</sup> –O <sup>2–</sup>  | 9547.96 | 0.2192 | 32                     | [13]      |

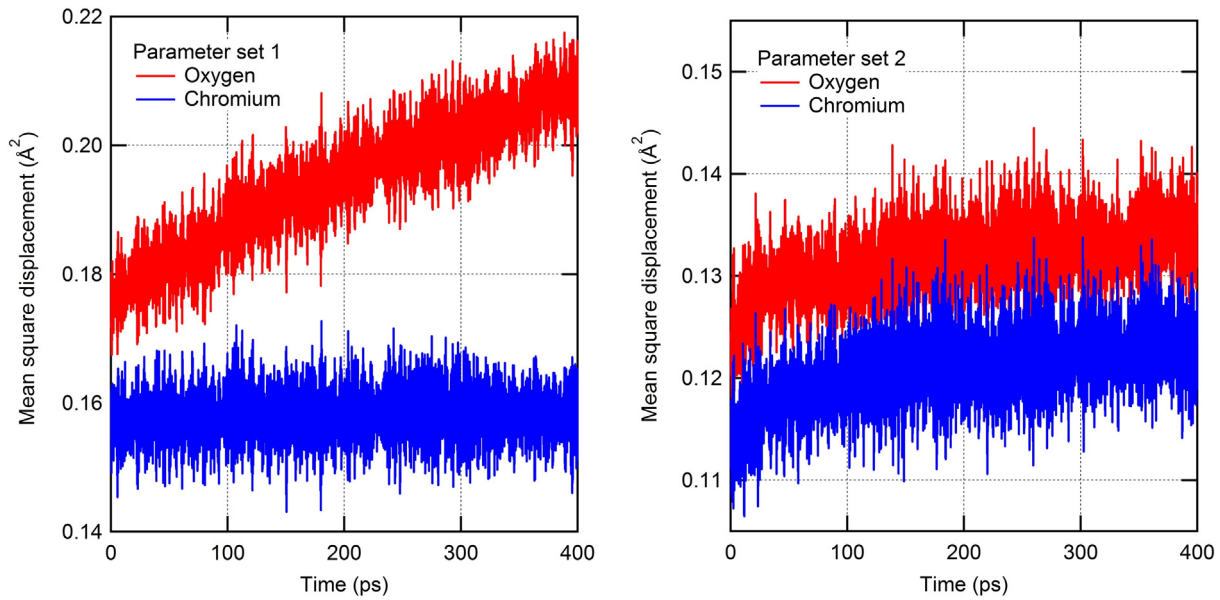


Fig. 2. Mean square displacement of oxygen and chromium ions in  $\alpha$ -Cr<sub>2</sub>O<sub>3</sub> for a Schottky defect concentration of  $8.3 \times 10^{-4}$  at a temperature of 1500 K. Left: Parameter set 1. Right: Parameter set 2.

for migration, but the values of Fe diffusion coefficient for parameter set 2 are two orders of magnitude larger. For oxygen, there are significant differences both in the values of the activation energy and the diffusion coefficient.

The Fe<sup>2+</sup> diffusion coefficients determined from the simulations for Fe<sub>3</sub>O<sub>4</sub> at a Schottky defect concentration of  $6.7 \times 10^{-4}$  are presented in Fig. 5. The migration activation energy for Fe<sup>2+</sup> in Fe<sub>3</sub>O<sub>4</sub> is similar to Fe<sup>3+</sup> in Fe<sub>2</sub>O<sub>3</sub>, but the value of the diffusion coefficient for Fe<sup>2+</sup> in Fe<sub>3</sub>O<sub>4</sub> is an order of magnitude larger than for Fe<sup>3+</sup> in Fe<sub>2</sub>O<sub>3</sub> (parameter set 2). The parameterization used for the interaction potential did not predict detectable diffusion for the Fe<sup>3+</sup> cation or oxygen. Experimentally, the majority defects in Fe<sub>3</sub>O<sub>4</sub> are believed to be either cation vacancies or interstitials, depending on oxygen partial pressure [16,17]. The diffusion of oxygen in Fe<sub>3</sub>O<sub>4</sub> has been studied by Millot and Niu [18], who determined the oxygen defects to be either free oxygen vacancies (low oxygen pressures) or anion–cation vacancy pairs (high oxygen pressures). The latter defect type was not included in this study. However, for oxygen vacancies, the MD results are at qualitative variance with experiments.

The diffusion coefficients determined from the simulations for FeCr<sub>2</sub>O<sub>4</sub> at a Schottky defect concentration of  $6.7 \times 10^{-4}$  are presented in Fig. 6. All ions are mobile, but Fe<sup>2+</sup> has the largest diffusion coefficient and the smallest activation energy for migration. The Fe<sup>2+</sup> data also show the largest scatter, which is attributed to the fact that only one ion out of seven is Fe<sup>2+</sup>, so the statistics is inherently worse compared to other ions. Here it is interesting to note the study by Nagata et al. [19] on FeCr<sub>2</sub>O<sub>4</sub> spinel formation in a FeO/Cr<sub>2</sub>O<sub>3</sub> interface. They attribute the spinel formation to Fe<sup>2+</sup> diffusion through spinel and subsequent reaction at spinel/Cr<sub>2</sub>O<sub>3</sub> interface. The bulk diffusion coefficients reported by Gilewicz-Wolter et al. [20] for Fe and Cr in FeCr<sub>2</sub>O<sub>4</sub> are close to each other.

The dependence of the oxygen diffusion coefficient on the defect concentration for  $\alpha$ -Cr<sub>2</sub>O<sub>3</sub> is presented in Fig. 7. It can be observed that the dependence seems to be close to linear for the three lower defect concentrations studied, but a deviation from linearity occurs when going to the highest defect concentration especially for temperatures between 1300 K and 1700 K. This suggest that at a defect concentration of  $8.3 \times 10^{-4}$ , the defects can no longer be regarded as completely isolated from each other. In particular, the possibility of two defects being initially close to each other increases, which gives

more freedom for the lattice to deform and allow atoms to diffuse. Marrocchelli et al. [21] studied defect-induced lattice expansion around oxygen vacancies in several fluorite-structured oxides, and from their molecular dynamics simulations, they concluded that vacancies start to significantly interact with each other above a critical concentration of  $2.5 \times 10^{-4}$ .

#### 4. Discussion

The diffusion coefficient can be expressed in the form

$$D = D_0 \exp\left(-\frac{E_A}{kT}\right) = D_0 \exp\left(-\frac{E_F + E_M}{kT}\right)$$

where  $E_A$  is the overall activation energy for diffusion and which contains contributions due to defect formation ( $E_F$ ) and migration ( $E_M$ ). The results of this study are directly concerned with  $E_M$ , since mechanisms and energetics of defect formation is not modeled. The implications of the  $E_M$  values for  $E_F$  are however discussed below.

Only few experimental studies were found in literature that concerned the activation energy for migration for the defect types and materials of this study. The activation energies for electronic and ionic diffusion in Cr<sub>2</sub>O<sub>3</sub> scales grown on Ni-20%Cr alloy were measured by Liu et al. [22] using asymmetry polarization technique. Whereas pure electronic conductivity was observed above 700 °C, mixed electronic and ionic conductivity was observed below 700 °C. The activation energies for electronic and ionic conductivities were 0.6 eV and 0.3 eV, respectively. The analysis by Liu et al. [22] assumes that chromium interstitials dominate the ionic conduction. However, the activation energy of 0.3 eV for ionic conduction is close to the activation energy of 0.37 eV found in Fig. 4 for Cr vacancy diffusion. Betova et al. [23] determined kinetic and transport parameters for the inner oxide layer on AISI 316 L(NG) stainless steel in temperature range of 150–300 °C using the mixed-conduction model [24] and found activation energies of 0.45 eV and 0.51 eV for chromium and iron diffusion, respectively.

Horita et al. [25] used an isotope tracer technique to study oxygen diffusion in the oxide scales formed on Fe-Cr-based ferritic stainless steels. The oxide scales consisted of a Fe-Mn spinel on top of a layer

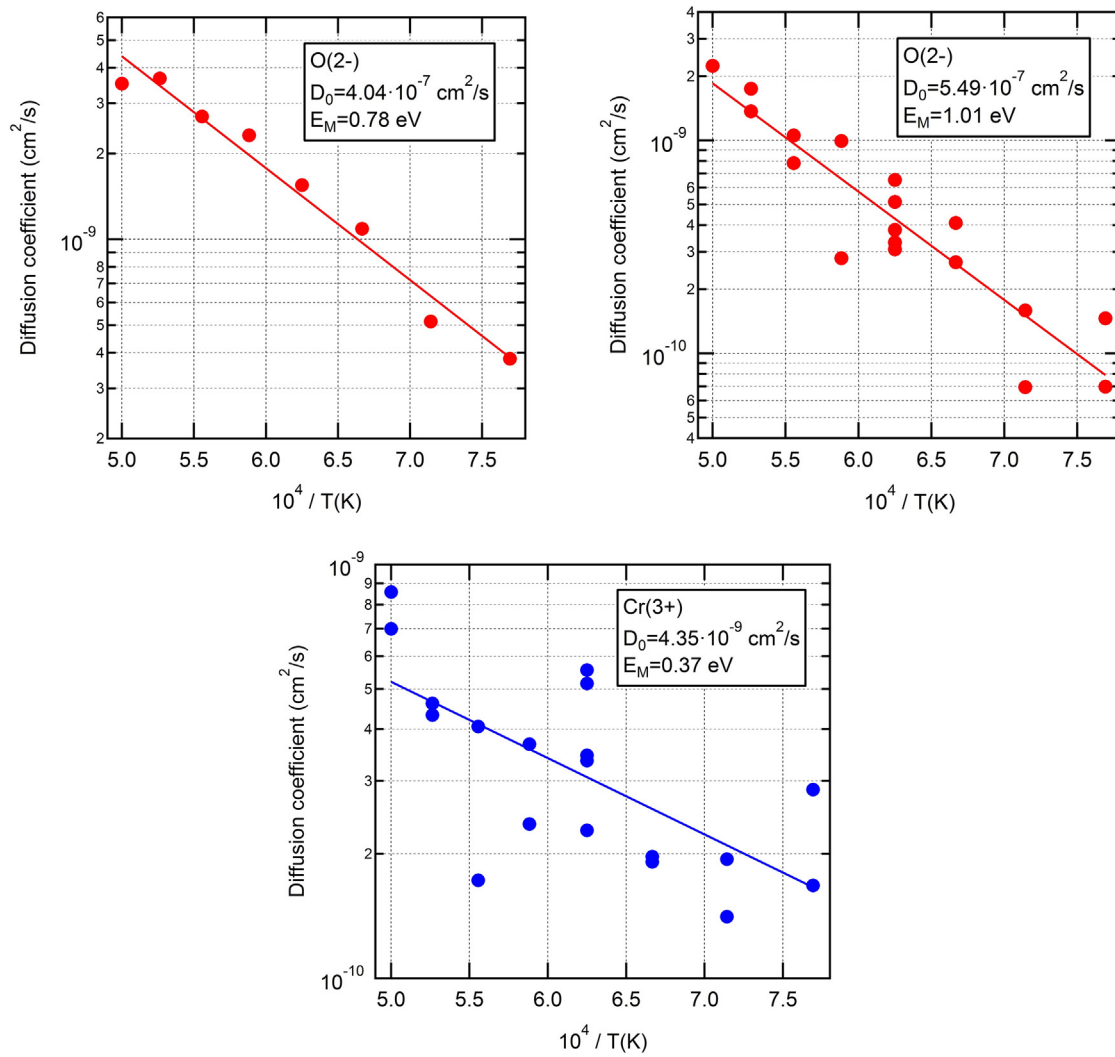


**Fig. 3.** Diffusion coefficients (markers), Arrhenius fits (lines) and Arrhenius parameters (annotations) for O and Cr diffusion in  $\alpha$ -Cr<sub>2</sub>O<sub>3</sub> for parameter sets 1 and 2 at a Schottky defect concentration of  $8.3 \times 10^{-4}$ . Top left:  $D_0$  for parameter set 1. Top right:  $D_0$  for parameter set 2. Bottom:  $D_{Cr}$  for parameter set 2.

described as ‘Cr-rich spinel or Cr<sub>2</sub>O<sub>3</sub>’. These authors found an activation energy of 1.4 eV for oxygen diffusion, somewhat larger than the value of 1.01 eV found for  $\alpha$ -Cr<sub>2</sub>O<sub>3</sub> in Fig. 3 for parameter set 2 and significantly larger than the value of 0.57 eV found for FeCr<sub>2</sub>O<sub>4</sub> in Fig. 6.

Temperature-dependent diffusion coefficients in Cr<sub>2</sub>O<sub>3</sub> have been reported by several authors. Kofstad and Lillerud [14] present a compilation of data from Hagel and Seybolt [26], Hagel [27], Lindner and Åkerström [28] and Walters and Grace [29]. These data can be fitted with the following expressions:

$$\begin{aligned} D_{Cr} &= 4.3 \cdot 10^3 \exp(-415(\text{kJ/mol})/RT) \text{ cm}^2/\text{s} \quad (\text{sintered samples}) \\ D_{Cr} &= 0.167 \exp(-255(\text{kJ/mol})/RT) \text{ cm}^2/\text{s} \quad (\text{hot-pressed samples}) \\ D_O &= 15.9 \exp(-422(\text{kJ/mol})/RT) \text{ cm}^2/\text{s} \end{aligned}$$

The difference in the  $D_{Cr}$  values between the two sample preparation methods illustrates the difficulties in obtaining consistent experimental data for diffusion coefficients. The same conclusion was later drawn by Tsai et al. [30], who noted that the experimental diffusion coefficients presented by various authors can vary by orders of magnitude.

Amami et al. [15] measured temperature dependent bulk diffusion coefficients in Fe<sub>2</sub>O<sub>3</sub> natural single crystals in the temperature range 890 to 1227 °C. Their data can be fitted as follows:

$$\begin{aligned} D_{Fe} &= 9.2 \cdot 10^{10} a(O_2)^{-0.56} \exp(-578(\text{kJ/mol})/RT) \text{ cm}^2/\text{s} \\ D_O &= 2.7 \cdot 10^8 a(O_2)^{-0.26} \exp(-542(\text{kJ/mol})/RT) \text{ cm}^2/\text{s} \end{aligned}$$

The activation energy for iron is close to 510 kJ/mol determined by Sabioni et al. [31] for their Fe<sub>2</sub>O<sub>3</sub> single crystal samples above 1200 K. It can be noted that the activation energies for diffusion are higher in Fe<sub>2</sub>O<sub>3</sub> single crystals as compared to Cr<sub>2</sub>O<sub>3</sub> samples prepared from powders.

Besides morphology, the issues connected to sample preparation are impurities whose role has been pointed out in several studies [3,6–9]. The computational work by Atkinson et al. [3] provides important insight into the energetics of defect formation due to impurities in  $\alpha$ -Al<sub>2</sub>O<sub>3</sub>,  $\alpha$ -Cr<sub>2</sub>O<sub>3</sub> and  $\alpha$ -Fe<sub>2</sub>O<sub>3</sub>. In particular, they find that aliovalent dopants with a small ionic radius in these materials (such as Mg<sup>2+</sup> or Ti<sup>4+</sup>) may have solution energies as low as about 2 eV, which are significantly lower than the formation energy of intrinsic defects. In addition, such doping will drive up the concentration of point defects through charge compensating reactions.



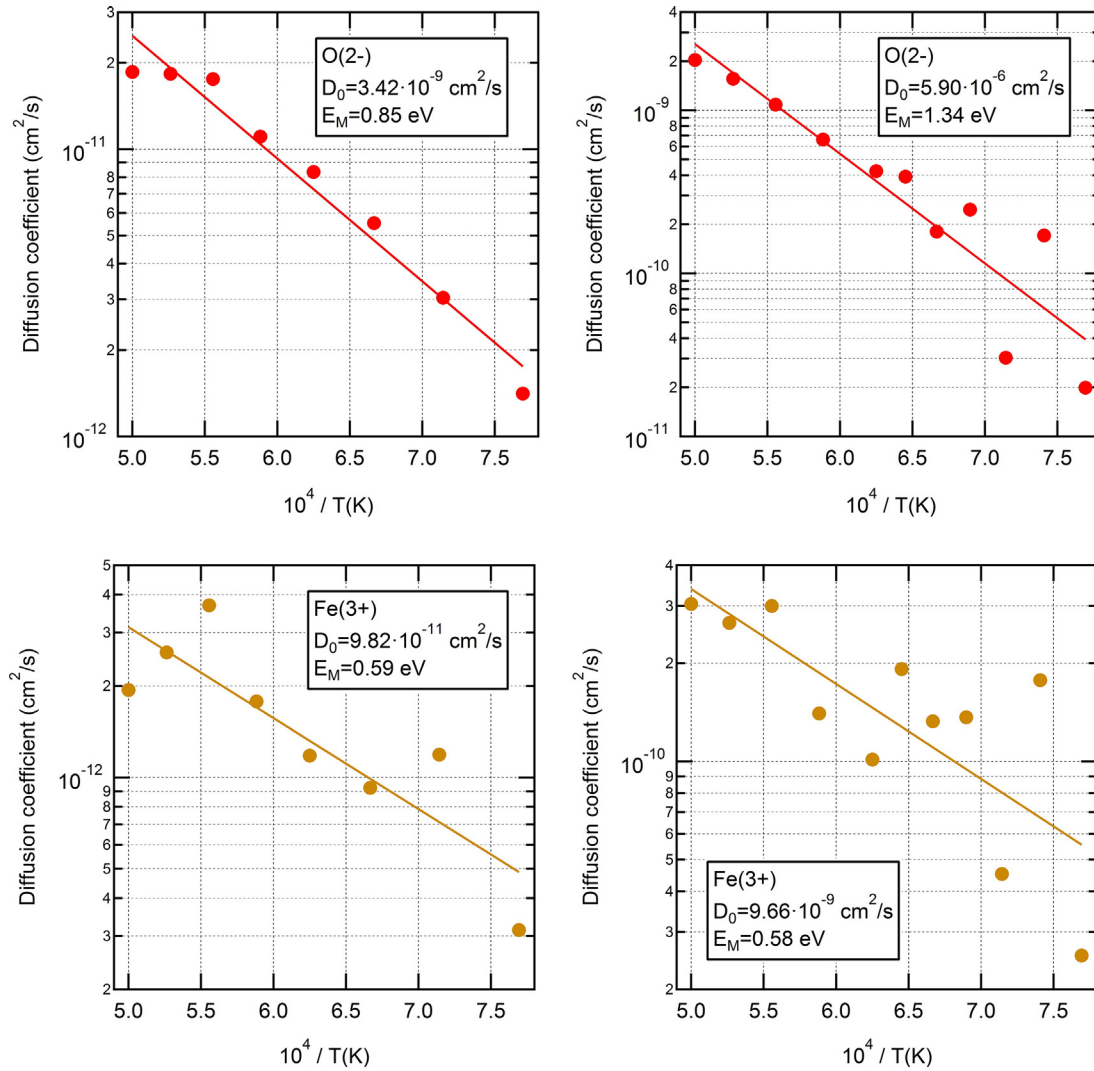


**Fig. 4.** Diffusion coefficients (markers), Arrhenius fits (lines) and Arrhenius parameters (annotations) for O and Fe diffusion in  $\alpha\text{-Fe}_2\text{O}_3$  for parameter sets 1 and 2 at a Schottky defect concentration of  $8.3 \times 10^{-4}$ . Top left:  $D_{\text{O}}$  for parameter set 1. Top right:  $D_{\text{O}}$  for parameter set 2. Bottom left:  $D_{\text{Fe}}$  for parameter set 1. Bottom right:  $D_{\text{Fe}}$  for parameter set 2.

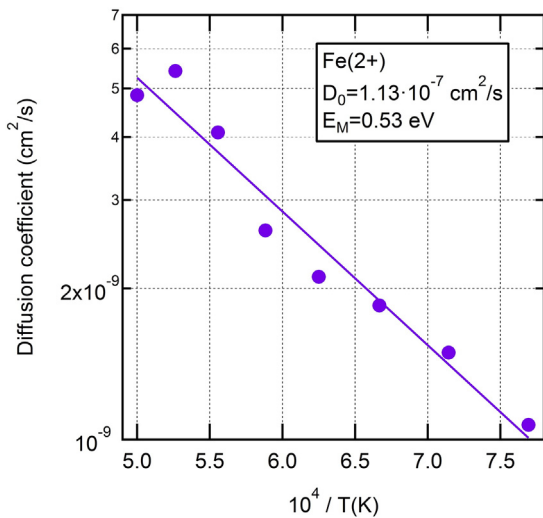


**Fig. 5.** Diffusion coefficients (markers), Arrhenius fit (line) and Arrhenius parameters (annotation) for  $\text{Fe}^{2+}$  diffusion in  $\text{Fe}_3\text{O}_4$  at a Schottky defect concentration of  $6.7 \times 10^{-4}$ .

Atkinson et al. [3] also report intrinsic defect energies for Schottky, anion Frenkel and cation Frenkel defects. For Schottky defects in  $\alpha\text{-Cr}_2\text{O}_3$ , this is 5.59 eV, which is in excess of an earlier estimate of 4.22 eV by Catlow et al. [2]. Considering now the activation energies appearing in the expression for the diffusion coefficients for Cr in  $\alpha\text{-Cr}_2\text{O}_3$ , and subtracting the migration activation energy for Cr obtained in this work (0.37 eV), we arrive at defect formation energies of 3.93 eV for sintered samples and 2.27 eV for hot-pressed samples. Similarly, from the oxygen data, we get a defect formation energy of 3.36 eV. These are substantially below the intrinsic defect energies, suggesting that impurities are dominating the defect structure in these materials.

The situation is somewhat different for natural  $\text{Fe}_2\text{O}_3$  single crystals. The activation energies for diffusion are close to the intrinsic Schottky defect energy of 5.82 eV [3]. The impurity levels in the natural single crystals were typically below 50 ppm for aliovalent impurities. Amami et al. [15] report an activation energy of 9.44 eV for Fe diffusion along grain boundaries, attributing the high value to segregation of the impurities to grain boundaries or dislocation walls.

Given the estimates on the defect formation energies, it is instructive to examine the defect concentrations that these suggest and to compare

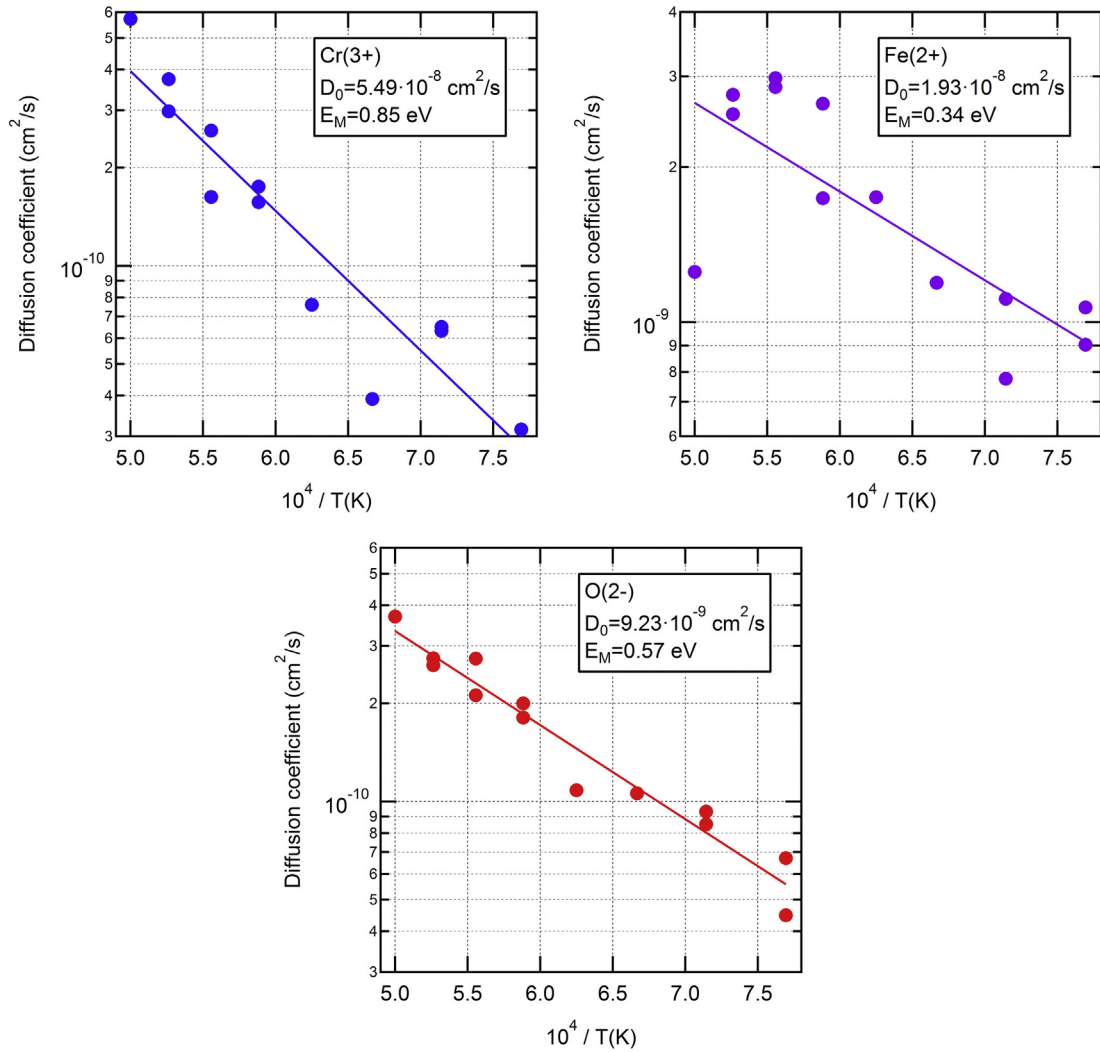


Fig. 6. Diffusion coefficients (markers), Arrhenius fits (lines) and Arrhenius parameters (annotations) for diffusion in  $\text{FeCr}_2\text{O}_4$  at a Schottky defect concentration of  $6.7 \times 10^{-4}$ .

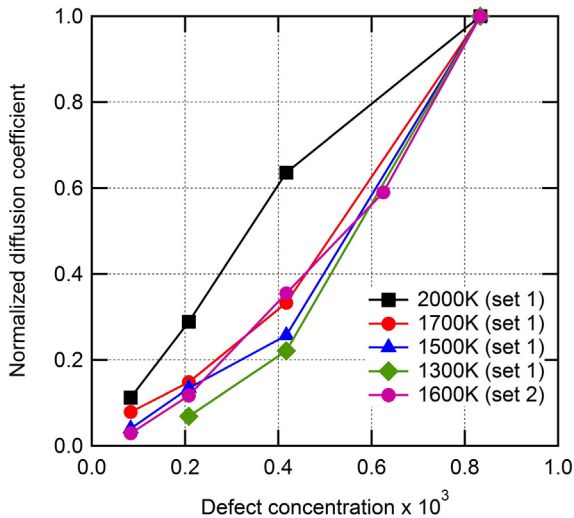


Fig. 7. Normalized oxygen diffusion coefficients as a function of Schottky defect concentration for  $\alpha\text{-Cr}_2\text{O}_3$ . Solid markers correspond to parameter set 1, and open markers to parameter set 2.

these to the ones used in this study. Generally, the point defect concentration in a bulk crystal is given by

$$n/N = \exp(-E_F/RT)$$

where  $n$  is the number of defects,  $N$  is the total number of lattice sites (or structural formula units) and  $E_F$  is the formation energy of an isolated defect (where we assume  $n \ll N$ ). Fig. 8 presents the equilibrium defect concentration as a function of temperature for selected values of  $E_F$ . When considering defect concentrations in real materials, it is important to understand the temperature history of the samples. For example, Holt and Kofstad [6] prepared their  $\text{Cr}_2\text{O}_3$  samples by first cold-pressing high-purity  $\text{Cr}_2\text{O}_3$  powder followed by either sintering for one hour at 1783 K or by hot-pressing at 1673 K for one hour. Whenever diffusion measurements are done at lower temperatures, it can be expected that the defect structure of the samples corresponds to the high-temperature conditions during sample preparation because diffusion processes in these materials are slow. Salomonsen et al. [32] suggest that in  $\text{Cr}_2\text{O}_3$ , the defect structure is "frozen in" below 1300 K but is equilibrated with the surroundings at higher temperature. Fig. 8 suggests that even for the lowest defect formation energies around 2 eV,

the point defect concentration remains below the ppm range for practical temperatures.

The defect concentrations used in this work were 2–4 orders of magnitude higher than the highest concentrations suggested by Fig. 8. As explained in conjunction with Fig. 2, this was necessary to detect enough diffusion events within the computational time available. On the other hand, it was desired that the defects were isolated from each other, which was probably not the case with the highest defect concentrations used (see Fig. 7). This means that a direct computational measurement of diffusion events in a crystal with realistic point defect concentrations is computationally challenging, if not impossible, for defects with a high formation energy and at low temperatures.

Assuming, however, that for isolated defects the overall diffusion coefficient is linearly proportional to the point defect concentration, it is possible to extrapolate the results to lower defect concentrations. To exemplify this, we employ the data by Tsai et al. [30], who determined Cr and O bulk and grain boundary diffusion constants at 1073 K and 1173 K from  $\text{Cr}_2\text{O}_3$  scales grown by oxidation on  $\text{Ni}_{70}\text{Cr}_{30}$  alloy. The experimental data are shown in Fig. 9 together with linear fits to the Arrhenius plots of Fig. 3 (parameter set 2), which are extended down to the experimental temperatures. It is stressed that the slope in the lines is entirely due to the activation energy for migration. There is no change in the defect concentration as a function of temperature.

It is seen that extrapolation of the MD data for a defect concentration of  $8.3 \times 10^{-4}$  (the highest defect concentration involved in this study) passes close to the experimental grain boundary diffusion coefficients. Decreasing the defect concentration to  $2.5 \times 10^{-6}$  makes the MD data pass close to the apparent diffusion coefficient data. In order to make the MD data pass close to the bulk diffusion data, the defect concentration needs to be decreased well below the ppm range, which is in line with the defect concentrations in Fig. 8.

Only a limited amount of information is available on the defect concentrations in the oxides relevant to this study. Young et al. [8] employed Seebeck measurements to obtain defect concentrations. In this case, the measured thermoelectric power ( $\varepsilon$ ) relates to the concentration of charge carriers ( $n$ ) through  $\varepsilon = (k/e)\ln(N/n)$ , where  $k$  is the Boltzmann constant and  $N$  is the density of states, which is taken equal to the number of cation sites. For p-type  $\text{Cr}_2\text{O}_3$  at temperatures below 1300 K, Young et al. find a thermoelectric power of 750  $\mu\text{V/K}$  corresponding to an electron hole concentration of  $2 \times 10^{-4}$  per cation site. Young et al. then assume that chromium vacancies are present in the p-type material. Since one vacancy in a triply charged lattice corresponds

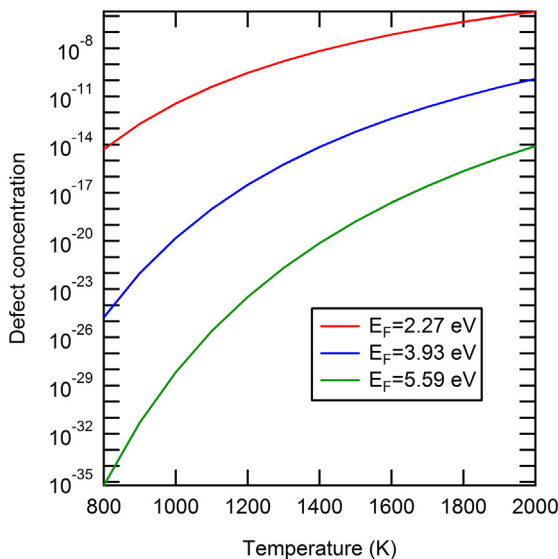


Fig. 8. Equilibrium concentration of point defects as a function of temperature for selected defect formation energies.

to three holes, they arrive at a defect concentration of  $6.7 \times 10^{-5}$ . Su and Simkovich [7] also applied Seebeck measurements to determine the point defect structure in pure and doped  $\text{Cr}_2\text{O}_3$ . At 1400 K temperature, they found a defect concentration of approximately  $1 \times 10^{-5}$ . These defect concentrations correspond to typical impurity levels in the low ppm range. In addition, the Seebeck measurements do not differentiate between charge carriers in the bulk and on grain boundaries. The defect concentration of  $2.5 \times 10^{-6}$  used in Fig. 9 to approximately reproduce the apparent diffusion coefficients is slightly below the values suggested by experiments.

## 5. Conclusions

Classical molecular dynamics simulations were used to gain insight into the relationship between the defect structure and the mass transport properties of  $\alpha\text{-Cr}_2\text{O}_3$ ,  $\alpha\text{-Fe}_2\text{O}_3$ ,  $\text{Fe}_3\text{O}_4$  and  $\text{FeCr}_2\text{O}_4$ . The focus in this study were Schottky defects, i.e., transport through lattice vacancies. Energetics and mechanisms of defect formation were not studied. Instead, pre-defined defect concentrations were used. Accordingly, the study yielded activation energies for migration in the case of vacancy diffusion.

Direct molecular dynamics simulations were conducted. Thermal noise and infrequency of transition events reduced the detection limit for diffusion coefficient to around  $10^{-12} \text{ cm}^2/\text{s}$ . This required the use of defect concentrations in the  $10^{-4}$  to  $10^{-3}$  range and temperatures in the 1300 K–2000 K range. These defect concentrations were higher than those expected in bulk material. The extrapolation of diffusion coefficients to lower defect concentrations was done by assuming that diffusion constants are linearly proportional to the defect concentration. Extrapolation of diffusion coefficients to lower temperatures was done through an Arrhenius plot.

Activation energies for migration were determined from the Arrhenius plots. For cations, these ranged between 0.37 eV and 0.91 eV, while for oxygen these ranged from 0.57 eV to 1.34 eV. For vacancy diffusion in  $\alpha\text{-Cr}_2\text{O}_3$  and  $\alpha\text{-Fe}_2\text{O}_3$ , cations were clearly more mobile than oxygen. For  $\text{FeCr}_2\text{O}_4$ , the mobility of the ions behaved as  $\text{Fe}^{2+} > \text{O}^{2-} > \text{Cr}^{3+}$ . For  $\text{Fe}_3\text{O}_4$ , only  $\text{Fe}^{2+}$  exhibited mobility that was detectable in the simulations.

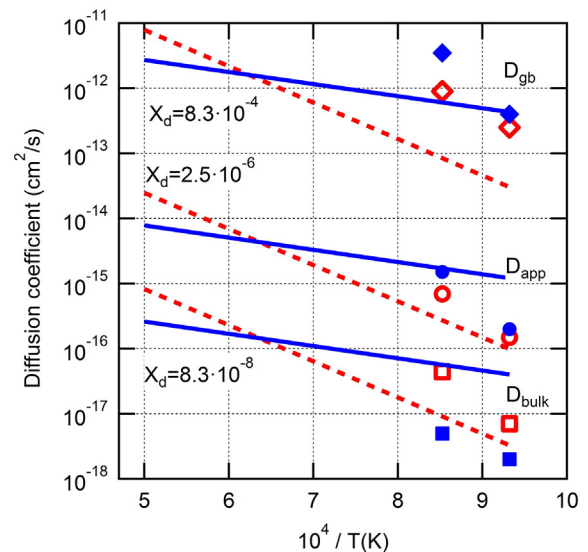


Fig. 9. Extrapolation of calculated Cr and O diffusion coefficients in  $\alpha\text{-Cr}_2\text{O}_3$  to lower temperatures and defect concentrations for parameter set 2 and for three different defect concentrations. The lines are the extended linear Arrhenius fits to Cr (solid lines) and O (dotted lines) data of Fig. 3. The markers are the experimental data by Tsai et al. (1996) for Cr (solid) and O (open) bulk diffusion (squares), grain boundary diffusion (diamonds) and apparent (spheres) diffusion coefficients.

For  $\alpha\text{-Cr}_2\text{O}_3$  and  $\alpha\text{-Fe}_2\text{O}_3$ , we showed that the results are sensitive to the Buckingham potential parameterization used. Especially for  $\alpha\text{-Cr}_2\text{O}_3$ , one parameter set resulted in oxygen mobility only, while another parameter set, both chromium and oxygen were mobile.

## References

- [1] D. Baxter, L. Heikinheimo (Eds.), Opticorr Guide Book. Optimization of in-service performance of boiler steels by modelling high-temperature corrosion, VTT Research Notes 2309VTT, Espoo, Finland 2005 (<http://www.vtt.fi/publications> (accessed 24.11.2014)).
- [2] C.R.A. Catlow, J. Corish, J. Hennessy, W.C. Mackrodt, J. Am. Ceram. Soc. 71 (1988) 42–49.
- [3] K.J.W. Atkinson, R.W. Grimes, M.R. Levy, Z.L. Coull, T. English, J. Eur. Ceram. Soc. 23 (2003) 3059–3070.
- [4] M.A. San Miguel, L.J. Álvarez, J.F. Sanz, J.A. Odriozola, J. Mol. Struct. (Theochem) 463 (1999) 185–190.
- [5] J. Sun, T. Stirner, A. Matthews, Surf. Sci. 601 (2007) 1358–1364.
- [6] A. Holt, P. Kofstad, Solid State Ionics 69 (1994) 127–136.
- [7] M.Y. Su, G. Simkovich, Technical Report No. TR 87-008, The Pennsylvania State University, Applied Research Laboratory 1987.
- [8] E.W.A. Young, J.H. Gerretsen, J.H.W. de Wit, J. Electrochem. Soc.: Solid-State Sci. Technol. 134 (1987) 2257–2260.
- [9] A. Holt, P. Kofstad, Solid State Ionics 100 (1997) 201–209.
- [10] S.J. Plimpton, J. Comput. Phys. 117 (1995) 1–19.
- [11] G.V. Lewis, C.R.A. Catlow, J. Phys. C Solid State Phys. 18 (1985) 1149–1161.
- [12] C.R.A. Catlow, Proc. R. Soc. A 353 (1977) 533–561.
- [13] L. Minervini, M.O. Zacate, R.W. Grimes, Solid State Ionics 116 (1999) 339–349.
- [14] P. Kofstad, K.P. Lillerud, J. Electrochem. Soc.: Solid-State Sci. Technol. 127 (1980) 2410–2419.
- [15] B. Amami, M. Addou, F. Millot, A. Sabioni, C. Monty, Ionics 5 (1999) 358–370.
- [16] S. Dorris, M. Martin, Ber. Bunsenges. Phys. Chem. 94 (1990) 721–726.
- [17] S. Aggarwal, J. Töpfer, T.-S. Tsai, R. Dieckmann, Solid State Ionics 101–130 (1997) 321–331.
- [18] F. Millot, Y. Niu, J. Phys. Chem. Solids 58 (1997) 63–72.
- [19] K. Nagata, R. Nishiwagi, Y. Nakamura, T. Maruyama, Solid State Ionics 49 (1991) 161–166.
- [20] J. Gilewicz-Wolter, Z. Zurek, J. Dudala, J. Lis, M. Homa, M. Wolter, Adv. Sci. Technol. 46 (2006) 27–31.
- [21] D. Marrocchelli, S.R. Bishop, J. Kilner, J. Mater. Chem. A 1 (2013) 7673–7680.
- [22] H. Liu, M.M. Stack, S.B. Lyon, Solid State Ionics 109 (1998) 247–257.
- [23] I. Betova, M. Bojinov, P. Kinnunen, T. Saario, VTT Research Report No VTT-R-04098-072007 (<http://www.vtt.fi/publications> (accessed 24.11.2014)).
- [24] B. Beverskog, M. Bojinov, A. Englund, P. Kinnunen, T. Laitinen, K. Mäkelä, T. Saario, P. Sirkkiä, Corros. Sci. 44 (2002) 1901–1921.
- [25] T. Horita, H. Kishimoto, K. Yamaji, Y. Xiong, M.E. Brito, H. Yokokawa, Y. Baba, K. Ogasawara, H. Kameda, Y. Matsuzaki, Solid State Ionics 179 (2008) 2216–2221.
- [26] W.C. Hagel, A.U. Seybolt, J. Electrochem. Soc.: Solid-State Sci. Technol. 108 (1961) 1146–1152.
- [27] W.C. Hagel, J. Am. Ceram. Soc. 48 (1965) 70–75.
- [28] R. Lindner, Å. Åkerström, Z. Phys. Chem. 6 (1956) 162–177.
- [29] L.C. Walters, R.E. Grace, J. Appl. Phys. 36 (1965) 2331.
- [30] S.C. Tsai, A.M. Huntz, C. Dolin, Mater. Sci. Eng. A212 (1996) 6–13.
- [31] A.C.S. Sabioni, A.M.J.M. Daniel, W.A.A. Macedo, M.D. Martins, A.M. Huntz, F. Jomard, A.I.C. Persiano, Defect Diff. Forum 237–240 (2005) 277–281.
- [32] G. Salomonsen, N. Norman, O. Lønsjø, T.G. Finstad, J. Phys. Condens. Matter 1 (1989) 7843–7850.